Nonperturbative beta function in three-dimensional electrodynamics

Ohad Raviv,[*] Yigal Shamir, and Benjamin Svetitsky

Raymond and Beverly Sackler School of Physics and Astronomy,
Tel Aviv University, 69978 Tel Aviv, Israel

We apply the Schrödinger functional method to the Abelian gauge theory in three dimensions with $N_f = 2$ four-component fermions. We find that the calculated beta function does not cross zero in the range of coupling we study. This implies that the theory exhibits confinement and mass generation, rather than a conformal infrared regime.

I. INTRODUCTION

The infrared structure of massless quantum electrodynamics in three dimensions (QED3) is an old problem [1]. Like other three-dimensional theories, QED3 is plagued by infrared divergences. It is widely believed that these signal a ground state that is far from the perturbative vacuum. Two possibilities have been entertained [2]. One is that the infrared physics of the theory is described by confinement of charge, with a concomitant dynamical mass for the fermions. The other is that dynamical charges screen the Coulomb interaction, so that charges at large distances interact via a power law potential. In the first case the scale of the theory's physics is presumably set by the coupling e^2, which has dimensions of mass. In the second case, there is no scale in the infrared physics, but rather an emergent conformal symmetry. A number of studies have concluded that confinement and mass generation occur if the number of (four-component) fermions, N_f, is small. It is clear, on the other hand, that in the large-N_f domain the theory is screened and conformal. Estimates of N_c, the critical value of N_f that divides the two domains, have varied widely in various analytical approaches [3–19] and lattice simulations [20–28] (for interim summaries see [2,28]).

We can explore this question via the renormalization group, guided by our knowledge of four-dimensional non-Abelian gauge theories. The running of the coupling $e^2(q)$ is governed by the beta function,

$$\frac{de^2}{d\log q} = N_f b_1 e^4/q + \cdots, \tag{1}$$

where $b_1 > 0$ is the one-loop coefficient. Upon defining a dimensionless coupling $g^2(q) = e^2/q$, we have

$$\frac{dg^2}{d\log q} = -g^2 + N_f b_1 g^4 + \cdots, \tag{2}$$

a form typical of a super-renormalizable field theory.[1] When N_f is small, there is a region around $g^2 = 0$ where the running is dominated by the first term, which has the sign associated with asymptotic freedom in four dimensions. As a consequence, the infrared running is towards strong coupling. When the coupling becomes large enough, but before the second term becomes important, a condensate $\langle \bar{\psi}\psi \rangle$ forms. This generates a mass for the fermions, whereupon at sufficiently small energy scales the fermions drop out of the theory, leaving free photons. The running of e^2 stops.

When N_f is large, on the other hand, the one-loop term in Eq. (2) has to be considered.[2] The beta function starts out negative at small g^2 but the one-loop term then makes it cross zero at $g^2 = g_*^2 \equiv (N_f b_1)^{-1}$. This is an infrared-attractive fixed point. Once the coupling runs there, a scale invariance sets in. There are no massive particles and indeed, since Green functions behave as powers of distance, there are no particles at all.

There must be a value of N_f, which we have called N_c, that divides the two domains. For N_f just below this N_c, the one-loop term is significant: It make the beta function turn towards zero as g^2 grows. This only happens, however, at a strong coupling, and the condensate is triggered before g^2 actually reaches the zero of the one-loop beta function. Then the fermions develop a mass and decouple in the infrared, as described for the small-N_f case.

These infrared scenarios are familiar from non-Abelian theories in four dimensions. In an asymptotically free theory the one-loop term in the beta function is negative, while the two-loop term changes sign as the number of fermion flavors is increased [29,30]. The transition from confinement to conformality has been much studied, most

---

[*]ohad.raviv@gmail.com

[1]b_1 depends on the renormalization scheme: It is not invariant under a perturbative change in scheme, $g^2 = g'^2 + bg'^4 + \cdots$. Hence we do not specify it further, until we adopt the Schrödinger functional scheme below. Since b_1 comes from screening by physical particles, it should be positive in any sensible scheme.

[2]In the 't Hooft limit, $N_f \to \infty$ with $e^2 N_f$ fixed, the one-loop term in Eq. (1) is the exact beta function.

recently by the methods of lattice gauge theory (for surveys see [31,32]).

The Schrödinger functional (SF) method gives a non-perturbative definition of the beta function that lends itself to lattice calculations [33,34]. Originally designed for QCD [35–37], it has also been applied to gauge theories that are on the borderline between confining and conformal [38–50]. In this paper we present a study of QED3 with $N_f = 2$ four-component fermions by this method. We first calculate and plot results for the beta function at fixed lattice spacing. These indicate that the beta function deviates from the one-loop form (2) at strong coupling and does not cross zero. This is confirmed when we extrapolate to the continuum by two different methods. Unless this trend is reversed at yet stronger couplings, our results imply that the $N_f = 2$ theory is a confining theory with a mass scale.

As mentioned above, more straightforward lattice methods have also been applied to QED3. We note in particular the extensive studies of Refs. [26–28]. This work has pointed towards $N_c \approx 2$. Calculating mass spectra and the chiral condensate is then quite challenging in the $N_f = 2$ theory, because of the strong finite-volume effects inherent in low dimensionality: If N_c is nearby then the condensate (if any) could be very small and particle masses (if any) likewise. Deciding whether these quantities are really nonzero requires simulation on very large lattices [14]. The strength of the SF method, on the other hand, comes from the idea behind the renormalization group. There is no need to control a large range of length scales in a given calculation, because the method relates nearby scales to derive the beta function. Thus finite size turns from a hindrance to a basis for calculation.

This paper is organized as follows. In Sec. II we review the SF method by adapting it to QED3; the language is entirely that of the continuum. We describe the lattice theory in Sec. III: a noncompact Abelian gauge field coupled to $N_f = 2$ four-component fermions. We simulate this theory to obtain the running coupling, with results presented in Sec. IV. Section V contains further discussion of our method, while the Appendices contain some technical details.

II. DEFINING THE RUNNING COUPLING

The Schrödinger functional offers a definition of the running coupling that is convenient for nonperturbative lattice calculations. We apply the method to QED3 in the continuum; lattice modifications will be given below. The action is

$$S = \int d^3x \left(\frac{1}{4e_0^2} F_{\mu\nu} F^{\mu\nu} + \sum_{i=1}^{N_f} \bar{\psi}_i \slashed{D} \psi_i \right), \quad (3)$$

where $F_{\mu\nu} = \partial_\mu A_\nu - \partial_\nu A_\mu$ is the usual field strength and $D_\mu = \partial_\mu + iA_\mu$. With this definition, A has dimensions of

mass and so does the coupling e_0^2. Renormalizing at a scale μ, we identify $e_0^2 \equiv e^2(\mu)$ and define a dimensionless coupling $g^2(\mu) = e^2(\mu)/\mu$.

We work in a cubic volume of size L^3 and impose a background field in a way that L is its only scale. Then calculation of the quantum effective action yields a coupling that runs with L, which we denote by $g^2(L)$.

We impose the background field through boundary conditions on the spacelike components A_x and A_y at $t = 0$ and $t = L$,

$$\begin{aligned} A_x = A_y &= +\phi/L, &\quad t &= 0, \\ A_x = A_y &= -\phi/L, &\quad t &= L. \end{aligned} \quad (4)$$

The background field in the bulk is found by minimizing the classical action,

$$S_{\text{cl}} = \frac{1}{e_0^2} \int d^3x \frac{1}{4} F_{\mu\nu} F^{\mu\nu}, \quad (5)$$

and it is easy to see that the solution is a linear function of t,

$$A_x(t) = A_y(t) = \frac{\phi}{L}\left(1 - \frac{2t}{L}\right), \quad (6)$$

corresponding to a constant electric field,

$$E_x = E_y = -\frac{2\phi}{L^2}. \quad (7)$$

The classical action of this field is

$$S_{\text{cl}} = \frac{4\phi^2}{e_0^2 L} \equiv \frac{\tilde{K}(\phi)}{e_0^2 L}. \quad (8)$$

In our work we fixed the background field parameter to be $\phi = \pi/4$.

The effective action $\Gamma = -\log Z$ gives a definition of the running coupling in the SF scheme. We write

$$\Gamma \equiv \frac{1}{e^2(L)} \int d^3x \frac{1}{4} F_{\mu\nu} F^{\mu\nu}, \quad (9)$$

where $F_{\mu\nu}$ is the classical background field. Using Eqs. (5) and (8) gives

$$\Gamma = \frac{\tilde{K}(\phi)}{e^2(L)L} = \frac{\tilde{K}(\phi)}{g^2(L)}, \quad (10)$$

and thus a calculation of Γ, in a three-dimensional volume of size L, gives directly the running coupling $g^2(L)$ at the scale L. In any field theory, one generally calculates not Γ but its derivatives, which are given by Green functions. Thus we differentiate with respect to the boundary parameter to obtain

$$\frac{\partial \Gamma}{\partial \phi} = \frac{K(\phi)}{g^2(L)}, \tag{11}$$

where $K = \partial \tilde{K} / \partial \phi$. (Our choice $\phi = \pi/4$ gives $K = 8\phi = 2\pi$.)

We can check our numerical results by comparing to the first two terms in a loop expansion for Γ,

$$\Gamma = S_{\text{cl}} + \Gamma^{(1)} + \cdots. \tag{12}$$

The one-loop quantum correction is given by

$$\Gamma^{(1)} = -N_f \text{tr} \, \log(\not{D}), \tag{13}$$

and thus we define the one-loop quantity $c(\phi)$ via

$$\frac{\partial \Gamma^{(1)}}{\partial \phi} \equiv N_f K(\phi) c(\phi). \tag{14}$$

[We have taken out a factor of $K(\phi)$ for convenience.] Here $c(\phi)$ is a dimensionless function of the boundary conditions, independent of the coupling and of the system size L. We calculate it in Appendix A. Inserting in Eq. (11) we have the perturbative expression for the running coupling,

$$\frac{1}{g^2(L)} = \frac{1}{g^2(\mu)\mu L} + N_f c + \cdots. \tag{15}$$

Setting $q = 1/L$, we rewrite the renormalization group equation (2) as

$$\tilde{\beta}(1/g^2) \equiv \frac{d(1/g^2)}{d \log L} = -\frac{1}{g^2} + N_f b_1 + O(g^2). \tag{16}$$

Upon differentiating Eq. (15), we identify

$$b_1 = c, \tag{17}$$

the one-loop coefficient in the SF renormalization scheme.

III. THE LATTICE THEORY

We use a noncompact formulation of the gauge field, wherein we define the vector potential $A_{n\mu}$ on each link (n, μ) of the three-dimensional lattice; we put a four-component Dirac field ψ_n on each site n. (We suppress the flavor index $f = 1, 2$ throughout.) The Euclidean action contains the usual quadratic term for the gauge field and a smoothed Wilson-clover action for the fermions,

$$S = \frac{\beta}{2} \sum_{\substack{n \\ \mu < \nu}} (\nabla \times A)_{n\mu\nu}^2 + \bar{\psi} D \psi. \tag{18}$$

All the fields in Eq. (18) have been made dimensionless via appropriate powers of the lattice spacing a. The lattice curl is

$$(\nabla \times A)_{n\mu\nu} = A_{n\mu} + A_{n+\hat{\mu},\nu} - A_{n+\hat{\nu},\mu} - A_{n\nu}, \tag{19}$$

and the first summation in Eq. (18) counts each plaquette once. The fermion term is

$$\bar{\psi} D \psi = \sum_n \bar{\psi}_n \psi_n \tag{20a}$$

$$+ \kappa \sum_{n\mu} [\bar{\psi}_n (1 + \gamma_\mu) V_{n\mu} \psi_{n+\hat{\mu}} + \bar{\psi}_{n+\hat{\mu}} (1 - \gamma_\mu) V_{n\mu}^\dagger \psi_n] \tag{20b}$$

$$+ \kappa c_{\text{SW}} \sum_n \bar{\psi}_n \frac{i}{4} \sigma_{\mu\nu} F_{n\mu\nu} \psi_n. \tag{20c}$$

The Wilson hopping term (20b) contains a link connection $V_{n\mu}$. This is constructed from the compact gauge variables

$$U_{n\mu} = e^{iA_{n\mu}} \tag{21}$$

by a normalized hypercubic (nHYP) smearing process [51,52], where each $V_{n\mu}$ is a weighted average of the U variables on nearby links (see Appendix B). The purpose of this smearing is the suppression of lattice artifacts. It allows us to go to stronger couplings before encountering numerical instabilities [46].

A further cancellation of lattice artifacts is offered by the clover term (20c) [53]. While the field strength $F_{n\mu\nu}$ could be defined via the simple curl (19), we adopt a definition appropriate to the compact theory, a sum over the four leaves of the "clover" surrounding the site n,

$$F_{n\mu\nu} = \frac{1}{4} (F_{n\mu\nu}^{(1)} + F_{n-\hat{\mu},\mu\nu}^{(1)} + F_{n-\hat{\nu},\mu\nu}^{(1)} + F_{n-\hat{\mu}-\hat{\nu},\mu\nu}^{(1)}), \tag{22}$$

where each term $F^{(1)}$ is a compact curl,

$$F_{n\mu\nu}^{(1)} = \sin(\nabla \times A)_{n\mu\nu}. \tag{23}$$

This clover structure is the same as in non-Abelian theories and enables easy adaptation of existing code. We set the coefficient to its tree-level value, $c_{\text{SW}} = 1$, since we have found this to be close to optimal when nHYP smearing is used [54].

The boundary conditions (4) for the Schrödinger functional are now imposed on the gauge field on the time slices of the lattice at $t = 0$ and $t = L$. Moreover, there are no dynamical fermion fields on these boundaries.

The coupling in Eq. (18) is

$$\beta = \frac{1}{e_0^2 a}, \tag{24}$$

where e_0 is the bare charge. The hopping parameter is related to the bare electron mass m_0 by

$$\kappa = \frac{1}{6 + 2m_0 a}. \tag{25}$$

We study the massless theory by demanding that the measured, physical fermion mass m vanish. We define this from the axial Ward identity,

$$\partial_\mu^- A_\mu^a = 2mP^a, \tag{26}$$

where $A_\mu^a = \frac{1}{2}\bar{\psi}\gamma_\mu\gamma_5\tau^a\psi$ is the isovector axial current and $P^a = \frac{1}{2}\bar{\psi}\gamma_5\tau^a\psi$ is the isovector pseudoscalar density. (∂_μ^- is the backward lattice derivative.) It is convenient in a SF calculation to define a gauge-invariant, pseudoscalar wall source operator $\mathcal{O}^a$ near the boundary at $t = 0$ (see Refs. [54,55] for details). Then Eq. (26) can be used to relate two Green functions at zero spatial momentum, viz.,

$$\partial_0^- \sum_{\mathbf{x}} \langle A_0^a(\mathbf{x},t)\mathcal{O}^a \rangle = 2m \sum_{\mathbf{x}} \langle P^a(\mathbf{x},t)\mathcal{O}^a \rangle. \tag{27}$$

We evaluate the Green functions at $t = L/2$, whence the ratio gives m. At each value of β, we tune the hopping parameter κ to make m vanish, which defines the critical curve $\kappa_c(\beta)$. We list the values of β used in this study, as well as the values of $\kappa_c(\beta)$, in Table I.

As mentioned above, a Monte Carlo simulation of the lattice theory does not give the effective action directly. Instead, one applies the Schrödinger functional method by using Green functions, which are derivatives of Γ. The derivative on the left-hand side of Eq. (11) is

$$\frac{\partial \Gamma}{\partial \phi}\bigg|_{\phi=\pi/4} = \left\langle \frac{\partial S_G}{\partial \phi} - \mathrm{tr}\left(\frac{1}{D^\dagger}\frac{\partial(D^\dagger D)}{\partial \phi}\frac{1}{D}\right) \right\rangle\bigg|_{\phi=\pi/4}, \tag{28}$$

where S_G is the pure gauge action, the first term in Eq. (18). Equation (28) is a particular expectation value of the gauge fields and the Dirac operator D. Differentiating with respect to ϕ is the same as differentiating with respect to $A_{n\mu}$ on the boundary. We also impose twisted spatial boundary conditions on the fermion fields [35], $\psi(x + L) = \exp(i\theta)\psi(x)$, with $\theta = \pi/5$ on both spatial axes.

We employed the hybrid Monte Carlo algorithm [56–58] in our simulations. The molecular dynamics integration was accelerated with an additional heavy pseudofermion field [59], multiple time scales [60], and a second-order Omelyan integrator [61]. Since the noncompact formulation allows gauge fluctuations in which $A_{n\mu}$ can wander to infinity, we monitor the field and carry out gauge transformations, local and global, to keep the field within certain bounds.

IV. THE RUNNING COUPLING AND THE BETA FUNCTION

We calculated the running coupling from Eqs. (11) and (28) for lattice sizes $L/a = 8$, 12, 16, and 24 for the bare couplings listed in Table I. The results are shown in Table II. We use different subsets of the data for two different analysis methods. Our goal is the beta function $\tilde{\beta}$, defined in Eq. (16), or, equivalently, its representation as the rescaled discrete beta function (RDBF) [47] for scaling by a fixed factor s,

$$R(u,s) \equiv \frac{u(sL) - u(L)}{\log s}, \tag{29}$$

where the argument is

$$u = u(L) \equiv \frac{1}{g^2(L)}. \tag{30}$$

It is clear that at a fixed point, where $\tilde{\beta} = 0$, the RDBF will be zero as well.

TABLE I. Summary of simulation runs for obtaining the running coupling g^2 at bare couplings (β, κ_c) for lattice sizes L used in this work. We used a trajectory length of unity for most of the simulations. The exceptions are the strong coupling runs ($\beta \leq 0.4$) and the $\beta = 0.6$ run on the biggest lattice, in which we used a trajectory length of $1/2$.

		Trajectories (thousands)			
β	κ_c	$L = 8a$	$L = 12a$	$L = 16a$	$L = 24a$
0.355	0.17440	150	150	$\cdots$	$\cdots$
0.39	0.17325	150	100	$\cdots$	$\cdots$
0.4	0.17282	100	150	150	122
0.458	0.17166	100	100	$\cdots$	$\cdots$
0.541	0.17055	100	100	$\cdots$	$\cdots$
0.6	0.16994	100	100	150	110
0.8	0.16898	100	100	100	100
1	0.16848	100	100	100	105
2	0.16757	$\cdots$	$\cdots$	50	50

TABLE II. Schrödinger functional running coupling calculated at bare couplings β on lattices of size L. The first two lines are affected by lattice artifacts that make them unusable in calculating the RDBF.

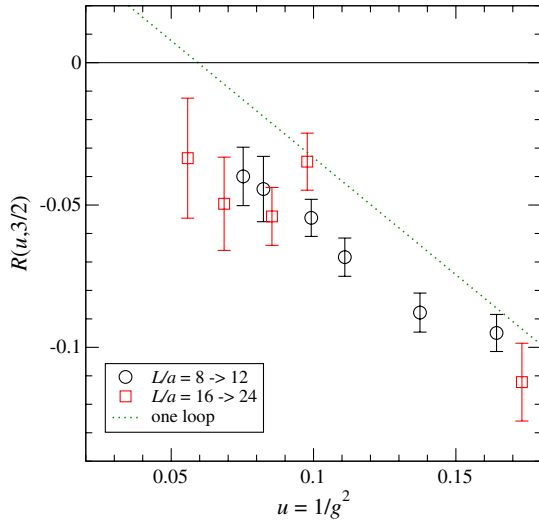|	$1/g^2$			
β	$L = 8a$	$L = 12a$	$L = 16a$	$L = 24a$
0.355	0.0753(20)	0.0515(35)	$\cdots$	$\cdots$
0.39	0.0751(18)	0.0608(42)	$\cdots$	$\cdots$
0.4	0.0753(24)	0.0591(34)	0.0558(41)	0.0422(75)
0.458	0.0824(22)	0.0644(41)	$\cdots$	$\cdots$
0.541	0.0992(16)	0.0771(21)	$\cdots$	$\cdots$
0.6	0.1110(16)	0.0833(22)	0.0686(21)	0.0485(63)
0.8	0.1374(17)	0.1018(22)	0.0854(26)	0.0635(32)
1	0.1643(16)	0.1258(21)	0.0978(25)	0.0837(32)
2	$\cdots$	$\cdots$	0.1732(35)	0.1277(43)

FIG. 1 (color online). The rescaled discrete beta function calculated from each pair of couplings for the lattices of size $L/a = 8 \to 12$ and $16 \to 24$.

A. Discrete beta function—two-lattice matching

We calculate the RDBF directly by comparing pairs of lattice sizes L and $L' = sL$ at fixed bare coupling β. [Two lattices with the same (β, κ) have the same lattice spacing.] Lattices of size $L = 8a$ and $12a$ give a scale factor $s = 3/2$, as do lattices of size $L = 16a$ and $24a$. We plot the RDBF for all such pairs of lattices in Fig. 1. For comparison we plot the one-loop formula, derived from using Eq. (15) in the definition (29),

$$R^{(1)}(u, s) = \frac{1 - 1/s}{\log s}(-u + N_f c). \qquad (31)$$

We note the general trend that as u decreases the data deviate downwards from the one-loop curve—away from the axis—and avoid its zero.

Figure 1 is a first look only, since the dependence on lattice spacing has not yet been studied. The quantity plotted in Fig. 1 is really $R(u, s; a)$, where the added argument is the lattice spacing. To extrapolate to $a = 0$, we seek data for R at fixed u—which means fixed L—but at different a, and thus different lattice size L/a. We show this procedure in Fig. 2. The horizontal lines link data points at fixed u, but measured on different lattice sizes $L/a = 8$ and $16.^3$ Thus the RDBFs calculated from these points are $R(u, s; a = L/8)$ and $R(u, s; a = L/16)$, respectively. We have such pairs at fixed u at $u \simeq 0.84$ and $u \simeq 0.98$. We replot them in Fig. 3, together with the extrapolations according to

---

[3]The points for $L = 8a$ were calculated at $\beta = 0.458$ and 0.541—lines 4 and 5 of Table II. These β values were chosen for this purpose, i.e., to match u to the $L = 16a$ values at $\beta = 0.8$ and 1.
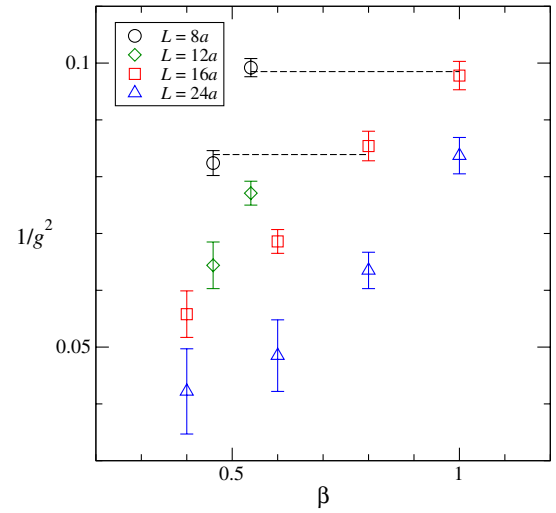

FIG. 2 (color online). Extrapolating the RDBF to the continuum. Plotted is a subset of the results for the running coupling that are listed in Table II. Pairs of data points at the same β give the RDBF for a single lattice spacing. The horizontal lines link data points at the same coupling $u = 1/g^2$ but at different lattice spacings. These pairs give the RDBF at the two lattice spacings, to be compared and extrapolated in Fig. 3.

$$R(u, s; a) = R(u, s; a = 0) + C\frac{a}{L}. \qquad (32)$$

It proved impossible to extend the two-lattice matching method to stronger coupling because of lattice artifacts. We attempted to extend the $L = 8a$ data to stronger couplings than those shown in Fig. 2 (see Table II). The measured coupling $1/g^2$ levels off, rather than continuing downward with smaller β. This prevents matching to the $L = 16a$ data.
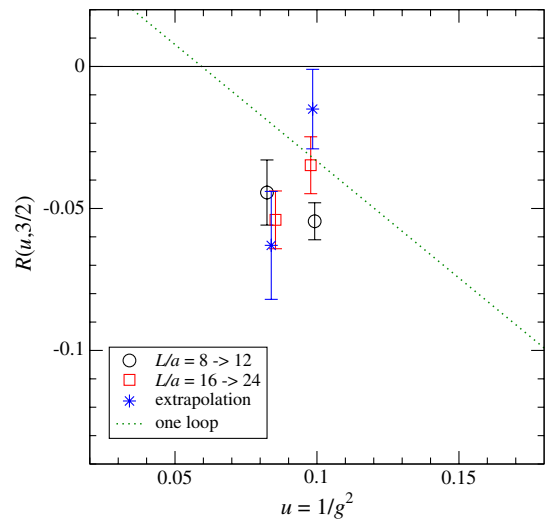

FIG. 3 (color online). Extrapolation of the RDBF to the continuum, at the two couplings for which we have the needed data.
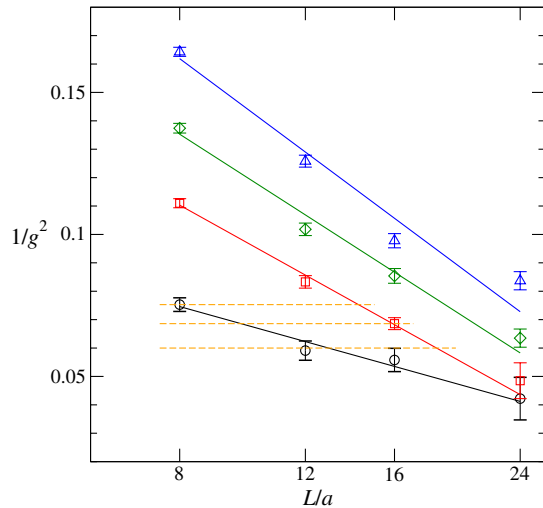
FIG. 4 (color online). Running couplings $1/g^2$ vs $\log(L/a)$, from Table II. Each set corresponds to a fixed bare coupling β. Top to bottom: $\beta = 1, 0.8, 0.6, 0.4$. The solid lines are the linear fits (33) for each bare coupling. The horizontal, dashed lines are values of $1/g^2$ chosen for extrapolating the slopes to $a/L = 0$.

B. Slope analysis

In order to perform an analysis at stronger couplings than the two-lattice method allows, we begin by plotting data sets for $1/g^2$ in Fig. 4. At four values of β, we have results for $1/g^2$ on four lattice volumes, $L = 8a, 12a, 16a$, and $24a$. Since fixing β fixes the lattice spacing a, these sets represent scaling in L at fixed a. As L is increased, $1/g^2$ decreases in accord with a negative beta function. The figure shows the results of a straight-line fit to each data set,

$$u(L) = \frac{1}{g^2(L)} = c_0 + c_1 \log L/a. \qquad (33)$$

At the two weakest bare couplings, $\beta = 1.0$ and 0.8, the fit is poor because of the obvious curvature of the dependence on $\log(L/a)$. This means that the decrease in $1/g^2$ is not described by a constant beta function $\tilde{\beta}$. Indeed, the one-loop continuum formula predicts that the decrease in $1/g^2$ slows as one moves leftward in Fig. 1.

At $\beta = 0.6$ and 0.4, on the other hand, a straight line fits the points well, with perhaps a small deviation for $L = 24a$ where the error bar is large anyway. Since g^2 is *not* constant as L changes, this motivates the hypothesis that the beta function $\tilde{\beta}(u)$ has leveled off in the range of u covered by these data. Thus we arrive at estimates $\tilde{\beta}(u) \simeq c_1$. The different slopes of the two data sets show that the estimates vary with the lattice spacing.

Choosing a value of $u = 1/g^2$ in Fig. 4 gives a horizontal line that intersects the fit lines for the two data sets. The two intercepts give two values of a/L, one for each fit. We again extrapolate these to the continuum linearly,

TABLE III. Extrapolation to $a/L = 0$ in slope analysis. $1/g^2$ is the chosen value of the running coupling for the horizontal line in Fig. 4. The next two columns are the values of L/a for the intercepts of the horizontal line with the fit lines for $\beta = 0.4$ and 0.6. The slopes for the two lines, which give $\tilde{\beta}(u; a)$, are respectively $-0.031(6)$ and $-0.062(4)$. The final column gives the extrapolation from these two values to $a/L = 0$ (Figs. 5 and 6).

$1/g^2$	$L/a(\beta = 0.4)$	$L/a(\beta = 0.6)$	$\tilde{\beta}(a/L \to 0)$
0.0753(24)	8	14.10(64)	$-0.103(13)$
0.0686(21)	9.73(87)	16	$-0.11(2)$
0.06	12.85(96)	18.04(65)	$-0.14(3)$

$$\tilde{\beta}(u; a) = \tilde{\beta}(u; a = 0) + C\frac{a}{L}, \qquad (34)$$

as shown in Table III and Fig. 5. The final result is plotted in Fig. 6.

The three u values chosen span a short interval. We do not go to yet stronger coupling in this analysis because lowering the chosen value of u in Fig. 4 will give intercepts that are too far to the right; here the data deviate from the straight lines, as they must, and the straight lines will not give accurate values of $\tilde{\beta}$.

[A complementary argument is the following. The quality of the linear fits in Fig. 4 is good for both $\beta = 0.4$ and 0.6. Therefore, when we extrapolate to the continuum limit it is legitimate to use the two slopes as estimates for the beta functions for any value $0.0422 \le u \le 0.0753$, which is the interval covered by the $\beta = 0.4$ data. (It is contained in the interval covered by
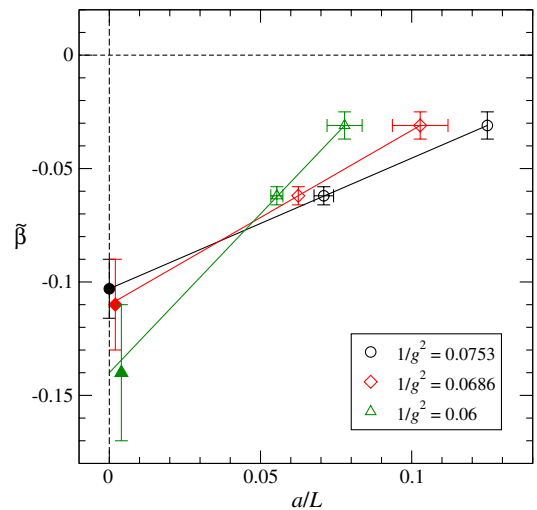

FIG. 5 (color online). Extrapolating the beta function to the continuum, as described in Table III. The y values of the upper and lower sets of data are the slopes of the fits shown in Fig. 4 for $\beta = 0.4$ and 0.6. The x values are the inverses of the intercepts of the horizontal lines in that figure with the fit lines. The data are extrapolated to $a/L = 0$ as shown (solid points, displaced horizontally from the axis for clarity).
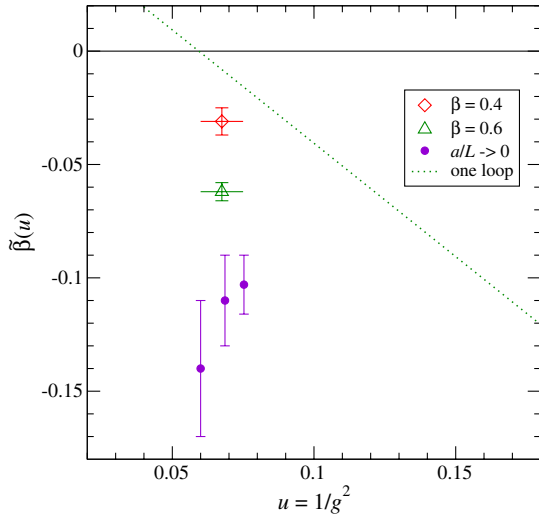
FIG. 6 (color online). Extrapolation of the beta function to the continuum (Table III and Fig. 5), plotted against the coupling. The points labeled $\beta = 0.4$ and 0.6 are the y values of the data plotted in Fig. 5. Assuming the slopes in Fig. 4 to be constant in the coupling range shown gives a set of extrapolations to $a/L = 0$, depending on the chosen value of u, as shown. The extrapolations are not statistically independent of each other.

the $\beta = 0.6$ data.) As we move down in u, however, the intercepts with the linear fits get closer to each other, and, moreover, the uncertainty in the L/a value of each intercept grows. As a result, the uncertainty in the continuum extrapolation grows rapidly, a trend that is clear in Figs. 5 and 6. Thus no further information will emerge from pushing to stronger coupling.]

Figure 6 shows that our numerical results deviate considerably from the one-loop curve. They show no sign of crossing the axis; taking Figs. 3 and 6 together, we have a beta function that approaches the axis with the one-loop curve but then curves away from it in the strong coupling region.

V. DISCUSSION

QED3 is qualitatively different from the four-dimensional non-Abelian theories studied with the SF method [38–50]. This is evident already in the weak-coupling behavior of the beta function. In four dimensions, the beta function $\tilde{\beta}(u)$ for the inverse coupling is constant in one loop; in three, it is linear in u, as seen in Eq. (16) and in the figures. Moreover, in the borderline-conformal theories there is a partial cancellation between the one-loop and two-loop terms that makes the beta function small compared to that of QCD. These differences are reflected in the analysis technique we adopt here, which is different from that in our earlier papers [47–50] and more closely resembles the applications of the method to QCD [37].

Our technique of linear fits at fixed bare coupling β [Eq. (33) and Fig. 4] was designed for a slowly running theory, where the slopes are small and the coupling changes

little from the smallest lattice to the largest. It works best when the beta function changes slowly as well. It is plain that neither property holds in Fig. 4: the slopes are large and the couplings change rapidly. For the two largest values of β, where the beta function is largest, the rate of change of the coupling decreases markedly as one follows the data to large volumes, so that the nonconstancy of the beta function is evident. At the smaller β's the slopes hold more nearly constant, validating the fits and allowing us to make the hypothesis that the beta function has leveled off.

We have used two different methods for extrapolation to the continuum, each with its own limitations. In weak coupling, we used the two-lattice method to extrapolate the rescaled discrete beta function. This works as long as one can match couplings between two different lattice sizes. As we saw, it fails at stronger couplings because of lattice artifacts. At the stronger bare couplings we use the fact that, as in QCD, the data in Fig. 4 cover overlapping ranges in the running coupling. The overlap between $\beta = 0.6$ and 0.4 allows for a straightforward extrapolation of the slope—the beta function—to $a/L = 0$.

It is evident from Fig. 4 that the slopes decrease as β decreases, as is to be expected from the form of the one-loop beta function. Thus the horizontal lines in Fig. 4 will associate the larger lattices (in terms of L/a) with larger slopes. It is then inevitable that extrapolating the slopes in Fig. 5 pushes the beta function away from the axis. Is the result, then, due more to our method than to the data? The examples offered by the four-dimensional non-Abelian theories show that this is not the case [47–50]. There, as one approaches a possible zero of the beta function, the slopes become so small that the fixed-β data sets do not overlap in coupling. This prevents an extrapolation of slopes to the continuum limit in those theories. An alternative method, based on only the linear fits at fixed β, leads to a beta function that stays near (or even crosses) zero [48].

ACKNOWLEDGMENTS

APPENDIX A: THE RUNNING COUPLING IN ONE LOOP

As explained in Sec. II, the one-loop coefficient in the beta function is given by $b_1 = c$, where
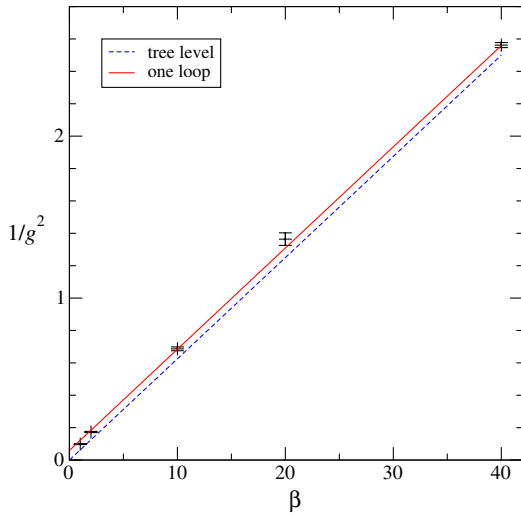
FIG. 7 (color online). Simulation results for $L = 16a$ in the weak-coupling regime compared to the calculated tree-level and one-loop expressions.

$$c = -\frac{1}{K}\frac{\partial}{\partial\phi}\log\det\mathcal{D}, \tag{A1}$$

which is to be evaluated at $\phi = \pi/4$, our choice for the SF boundary conditions.

The calculation of the derivative of the fermion determinant using the lattice regularization follows closely Ref. [35]. Since $\mathcal{D}$ is defined in a uniform (but time-dependent) background potential (6), its eigenfunctions take the form

$$\psi_\alpha(n) = \exp\left(i\mathbf{p}\cdot\mathbf{x}\right)f_\alpha(t), \tag{A2}$$

where $\mathbf{p} = (p_1, p_2)$, and α is a Dirac index. The allowed spatial momenta are

$$p_k = (2\pi n_k + \theta)/L, \qquad k = 1, 2, \tag{A3}$$

where θ is the fermion twist angle, and $n_k = 1, \ldots, \ell$, with $\ell = L/a$. Thus the calculation is reduced to

$$c = -\frac{1}{K}\lim_{\ell\to\infty}\sum_{\mathbf{p}}\frac{\partial}{\partial\phi}\log\det\tilde{\mathcal{D}}(\mathbf{p}), \tag{A4}$$

where $\tilde{\mathcal{D}}(\mathbf{p})$ is a $4(\ell - 1) \times 4(\ell - 1)$ matrix acting on functions of time $f_\alpha(t)$. (We recall that in the SF setup, the dynamical fermionic degrees of freedom live on time slices $t/a = 1, \ldots, \ell - 1$.) As shown in Ref. [35], one can simplify this expression to

$$\frac{\partial}{\partial\phi}\log\det\tilde{\mathcal{D}} = \mathrm{Tr}\left(M^{-1}\frac{\partial}{\partial\phi}M\right), \tag{A5}$$

where $M = M(\mathbf{p})$ is a 2×2 matrix that encodes the hopping in the time direction. For a fixed lattice of size ℓ, the calculation proceeds by using Eq. (A5) and summing over all $\mathbf{p}$. Thanks to the clover term, the result rapidly tends to a constant as L is increased, and we find

$$c = 0.0297(1). \tag{A6}$$

A comparison of the one-loop calculation with lattice simulations at very weak bare coupling is shown in Fig. 7. There is good agreement between the simulation results and the one-loop expression

$$\frac{1}{g^2(L)} = \frac{\beta}{\ell} + N_f c. \tag{A7}$$

APPENDIX B: nHYP SMEARING FOR THE ABELIAN THEORY

We modify the formulas of nHYP smearing [49,51,52] for the U(1) gauge group. While the smearing could be simplified by using the noncompact gauge field $A_{n\mu}$, we can take advantage of our experience with non-Abelian theories (as well as of existing code) by modifying the non-Abelian formulas to use the compact field $U_{n\mu}$. The reduction in dimensionality to three shortens the smearing procedure. The smeared links $V_{n\mu}$ are constructed from the bare links $U_{n\mu}$ in two consecutive smearing steps via intermediate fields $\tilde{V}$ according to

$$V_{n\mu} = \mathrm{Norm}\left[(1 - \alpha_1)U_{n\mu} + \frac{\alpha_1}{4}\sum_{\pm\nu\neq\mu}\tilde{V}_{n\nu;\mu}\tilde{V}_{n+\hat{\nu},\mu;\nu}\tilde{V}^\dagger_{n+\hat{\mu},\nu;\mu}\right], \tag{B1a}$$

$$\tilde{V}_{n\mu;\nu} = \mathrm{Norm}\left[(1 - \alpha_2)U_{n\mu} + \frac{\alpha_2}{2}\sum_{\pm\eta\neq\nu,\mu}U_{n\eta}U_{n+\hat{\eta},\mu}U^\dagger_{n+\hat{\mu},\eta}\right]. \tag{B1b}$$

Each step is a weighted averaging of a link with staples surrounding it. The restricted sums ensure that only links that share a cube with $U_{n\mu}$ enter the smearing. We set the parameters $\alpha_{1,2} = (0.75, 0.6)$ as used in Refs. [51,52] for the four-dimensional theory (where there is an additional direction in which to smear). The normalizations indicated in Eq. (B1) are simply

$$\mathrm{Norm}\,V = \frac{V}{|V|}. \tag{B2}$$

[1] R. D. Pisarski, Phys. Rev. D 29, 2423 (1984).
[2] T. Appelquist and L. C. R. Wijewardhana, arXiv:hep-ph/0403250.
[3] T. W. Appelquist, M. J. Bowick, D. Karabali, and L. C. R. Wijewardhana, Phys. Rev. D 33, 3704 (1986).
[4] T. Appelquist, D. Nash, and L. C. R. Wijewardhana, Phys. Rev. Lett. 60, 2575 (1988).
[5] D. Nash, Phys. Rev. Lett. 62, 3024 (1989).
[6] M. R. Pennington and D. Walsh, Phys. Lett. B 253, 246 (1991).
[7] D. C. Curtis, M. R. Pennington, and D. Walsh, Phys. Lett. B 295, 313 (1992).
[8] T. Appelquist, J. Terning, and L. C. R. Wijewardhana, Phys. Rev. Lett. 75, 2081 (1995).
[9] T. Ebihara, T. Iizuka, K.-i. Kondo, and E. Tanaka, Nucl. Phys. B434, 85 (1995).
[10] P. Maris, Phys. Rev. D 54, 4049 (1996).
[11] I. J. R. Aitchison, N. E. Mavromatos, and D. McNeill, Phys. Lett. B 402, 154 (1997).
[12] V. P. Gusynin, V. A. Miransky, and A. V. Shpagin, Phys. Rev. D 58, 085023 (1998).
[13] T. Appelquist, A. G. Cohen, and M. Schmaltz, Phys. Rev. D 60, 045003 (1999).
[14] V. P. Gusynin and M. Reenders, Phys. Rev. D 68, 025017 (2003).
[15] C. S. Fischer, R. Alkofer, T. Dahm, and P. Maris, Phys. Rev. D 70, 073007 (2004).
[16] K. Kaveh and I. F. Herbut, Phys. Rev. B 71, 184519 (2005).
[17] A. Bashir, A. Raya, I. C. Cloet, and C. D. Roberts, Phys. Rev. C 78, 055201 (2008).
[18] T. Goecke, C. S. Fischer, and R. Williams, Phys. Rev. B 79, 064513 (2009).
[19] J. Braun, H. Gies, L. Janssen, and D. Roscher, arXiv:1404.1362 [Phys. Rev. D (to be published)].
[20] E. Dagotto, J. B. Kogut, and A. Kocić, Phys. Rev. Lett. 62, 1083 (1989).
[21] E. Dagotto, A. Kocić, and J. B. Kogut, Nucl. Phys. B334, 279 (1990).
[22] V. Azcoiti and X.-Q. Luo, Mod. Phys. Lett. A 08, 3635 (1993).
[23] J. Alexandre, K. Farakos, S. J. Hands, G. Koutsoumbas, and S. E. Morrison, Phys. Rev. D 64, 034502 (2001).
[24] D. Lee and P. Maris, Phys. Rev. D 67, 076002 (2003).
[25] R. Fiore, P. Giudice, D. Giuliano, D. Marmottini, A. Papa, and P. Sodano, Phys. Rev. D 72, 094508 (2005); 72, 119902 (E) (2005).
[26] S. J. Hands, J. B. Kogut, and C. G. Strouthos, Nucl. Phys. B645, 321 (2002).
[27] S. J. Hands, J. B. Kogut, L. Scorzato, and C. G. Strouthos, Phys. Rev. B 70, 104501 (2004).
[28] C. Strouthos and J. B. Kogut, Proc. Sci, LAT2007 (2007) 278 [arXiv:0804.0300].
[29] W. E. Caswell, Phys. Rev. Lett. 33, 244 (1974).
[30] T. Banks and A. Zaks, Nucl. Phys. B196, 189 (1982).
[31] E. T. Neil, Proc. Sci., LATTICE2011 (2011) 009 [arXiv:1205.4706].
[32] J. Giedt, Proc. Sci., LATTICE2012 (2012) 006.
[33] M. Lüscher, R. Narayanan, P. Weisz, and U. Wolff, Nucl. Phys. B384, 168 (1992).
[34] M. Lüscher, R. Sommer, P. Weisz, and U. Wolff, Nucl. Phys. B413, 481 (1994).
[35] S. Sint and R. Sommer, Nucl. Phys. B465, 71 (1996).
[36] K. Jansen and R. Sommer (ALPHA Collaboration), Nucl. Phys. B530, 185 (1998); B643, 517(E) (2002).
[37] M. Della Morte, R. Frezzotti, J. Heitger, J. Rolf, R. Sommer, and U. Wolff (ALPHA Collaboration), Nucl. Phys. B713, 378 (2005).
[38] T. Appelquist, G. T. Fleming, and E. T. Neil, Phys. Rev. Lett. 100, 171607 (2008); 102, 149902(E) (2009).
[39] T. Appelquist, G. T. Fleming, and E. T. Neil, Phys. Rev. D 79, 076010 (2009).
[40] A. J. Hietanen, K. Rummukainen, and K. Tuominen, Phys. Rev. D 80, 094504 (2009).
[41] F. Bursa, L. Del Debbio, L. Keegan, C. Pica, and T. Pickup, Phys. Rev. D 81, 014505 (2010).
[42] F. Bursa, L. Del Debbio, L. Keegan, C. Pica, and T. Pickup, Phys. Lett. B 696, 374 (2011).
[43] M. Hayakawa, K.-I. Ishikawa, Y. Osaki, S. Takeda, S. Uno, and N. Yamada, Phys. Rev. D 83, 074509 (2011).
[44] T. Karavirta, J. Rantaharju, K. Rummukainen, and K. Tuominen, J. High Energy Phys. 05 (2012) 003; Proc. Sci., LATTICE2011 (2011) 067.
[45] Y. Shamir, B. Svetitsky, and T. DeGrand, Phys. Rev. D 78, 031502 (2008).
[46] T. DeGrand, Y. Shamir, and B. Svetitsky, Phys. Rev. D 82, 054503 (2010).
[47] T. DeGrand, Y. Shamir, and B. Svetitsky, Phys. Rev. D 83, 074507 (2011).
[48] T. DeGrand, Y. Shamir, and B. Svetitsky, Phys. Rev. D 87, 074507 (2013).
[49] T. DeGrand, Y. Shamir, and B. Svetitsky, Phys. Rev. D 85, 074506 (2012).
[50] T. DeGrand, Y. Shamir, and B. Svetitsky, Phys. Rev. D 88, 054505 (2013).
[51] A. Hasenfratz and F. Knechtli, Phys. Rev. D 64, 034504 (2001).
[52] A. Hasenfratz, R. Hoffmann, and S. Schaefer, J. High Energy Phys. 05 (2007) 029.
[53] B. Sheikholeslami and R. Wohlert, Nucl. Phys. B259, 572 (1985).
[54] Y. Shamir, B. Svetitsky, and E. Yurkovsky, Phys. Rev. D 83, 097502 (2011).
[55] M. Luscher, S. Sint, R. Sommer, and P. Weisz, Nucl. Phys. B478, 365 (1996).
[56] S. Duane and J. B. Kogut, Phys. Rev. Lett. 55, 2774 (1985).
[57] S. Duane and J. B. Kogut, Nucl. Phys. B275, 398 (1986).
[58] S. A. Gottlieb, W. Liu, D. Toussaint, R. L. Renken, and R. L. Sugar, Phys. Rev. D 35, 2531 (1987).
[59] M. Hasenbusch, Phys. Lett. B 519, 177 (2001).
[60] C. Urbach, K. Jansen, A. Shindler, and U. Wenger, Comput. Phys. Commun. 174, 87 (2006).
[61] T. Takaishi and P. de Forcrand, Phys. Rev. E 73, 036706 (2006).
[62] http://www.physics.utah.edu/~detar/milc/.
[63] A. Hasenfratz, R. Hoffmann, and F. Knechtli, Nucl. Phys. B, Proc. Suppl. 106–107, 418 (2002).